Analysis of silt behavior induced by water waves

LIN Mian (林 缅)

Institute of Mechanics, Chinese Academy of Sciences, Beijing 100080, China (email: linmian@mail.imech.ac.cn)
Received May 5, 2000

Abstract Based on the weak non-elastic porous model, the expressions of pore pressure, effective stress and displacements of soil skeletal frame and pore water have been deduced for a finite depth seabed. The distributions of several physical parameters have been analyzed for three kinds of marine sediment, including pore pressure, effective stress, stress angle, displacement of skeletal frame and pore fluid, and the variations of elastic waves with wave period. According to the experimental results, the resonant phenomena in the silt bed and the mechanism underlying such events have been discussed. It is proposed that the existence of a stiff soil layer inside the silt bed is a necessary condition for resonance to occur, and the possible location of resonance can be forecasted.

Keywords: **marine soil, stiffness layer, resonance.**

In many cases of coastal engineering, e.g. constructions of coastal structures, flotation of buried pipelines, etc. correct estimations of the dynamic behavior of seabed soil are very important. As ocean waves propagate over the seabed, the pore pressure and effective stresses in the marine sediments experience changes and give rise to a wide variety of phenomena. Many of these phenomena are complex and the associated physical mechanisms are not fully understood. As we know, the sediment consists of many pores or cavities, whose sizes primarily depend on the size distributions of the sediment, and whose structures determine their physics properties. Goddard[1] has found that, as some solid particles surrounding the soil skeletal frame would peel off under the external vibration stress, large pores may be formed in the soil. Bennett[2] has reported that the content of finer particles with particle sizes less than 62.5 μm within a cohesionless seabed can significantly influence the physical properties of marine soil. The laboratory wave flume measurements by Foda[3] and Tzang[1)] have shown that the pore water pressures in both sandy and silt seabed are very different. The pore pressure in sandy seabed shows a linear response to loading waves. However, the results from silty seabed have significantly large pressure oscillations. Sometimes, a resonance stage was identified, and fluidization of some degree took place inside the soil, leading to the ejection of soil particles from within the bed into the overlying water column. As a result, the seabed was eroded and sank.

Generally speaking, the dynamic behaviors induced by water waves are different for sand and silt seabeds. In particular, the fine sand or clay seabeds are mainly distributed over coastal areas. Therefore, it is worthwhile to study the dynamic behavior of silt in order to protect harbor environments and keep ocean structures stable. Because the response of pore pressure to loading waves in the silt seabed appear linear before resonance, the weak non-elastic model is applied

1) Tzang S. -Y., Water wave-induced soil fluidization in a cohesionless fine-grained, Ph.D. Dissertation, Department of Civil Engineering, University of California, Berkeley, 1992.

first in this paper[4]. The distribution of pore pressure, effective stresses and displacements of soil skeletal frame and pore water in the seabed are deduced. Moreover, the dynamic properties of the silt seabeds have been studied systematically based on experimental data[1, 3].

1 Theoretical model

1.1 Governing equations

The loading wave is assumed to propagate in the x-direction, the water-soil interface is defined as the origin of the xz plane, and the z-axis is positive upward from the water-soil interface and negative downward. The loading wave amplitude is regarded as small and the velocity potential, which satisfies the Laplace equation and the free surface boundary condition, can be written as

$$\varphi = \mathrm{i}a_0 g\{\cosh[\tilde{k}(z-h)]/\omega + \omega\sinh[\tilde{k}(z-h)]/g\tilde{k}\}\mathrm{e}^{\mathrm{i}(\omega t-\tilde{k}x)},$$

in which a_0 is the wave amplitude, $\tilde{k} = k_r + ik_i$ the complex wave number, ω the wave frequency, h the water depth, and g the gravitational constant. The seabed is considered as a porous elastic media with finite depth, homogeneous, isotropic, and with a compressible skeletal frame and pore fluid. The motion of the pore fluid relative to the skeletal frame is assumed to obey Darcy's law. Then the equations of motion of marine soil frame and pore fluid can be given as[5]

$$\begin{aligned}\frac{\partial^2}{\partial t^2}(\rho\boldsymbol{u} + \rho_f\boldsymbol{w}) &= \tilde{\mu}\nabla\boldsymbol{u} + (\tilde{H}-\tilde{\mu})\nabla e - \tilde{C}\nabla\zeta,\\ \frac{\partial^2}{\partial t^2}(\rho_f\boldsymbol{u} + m\boldsymbol{w}) + \frac{\eta_f}{k_s}\frac{\partial\boldsymbol{w}}{\partial t} &= \nabla(\tilde{C} - \tilde{M}\zeta),\end{aligned} \tag{1}$$

where η_f is the viscosity of the pore fluid, k_s the hydraulic coefficient of permeability of soil, $\tilde{\mu} = G(1 + i\delta)$ the complex shear modulus and given by the elastic modulus, G, and specific loss of energy δ; $\tilde{H}$, $\tilde{C}$ and $\tilde{M}$ denote Biot's[6] complex elastic moduli of porous media, and are derived using physical parameters of soil, $\rho = (1-\beta)\rho_r + \beta\rho_f$ is the bulk density of soil, ρ_r and ρ_f are densities of grain and fluid respectively, β is the porosity of the soil; the quantity $m = \frac{\rho_f}{\beta}(1 + \alpha)$ is the virtual mass of soil skeletal frame in the accelerated flow field, α is the added mass coefficient of the skeletal frame; ζ is defined as $\zeta = -\nabla\cdot\boldsymbol{w}$, where $\boldsymbol{w} = \beta(\boldsymbol{U} - \boldsymbol{u})$, $\boldsymbol{U}(U_x, U_y)$ and $\boldsymbol{u}(u_x, u_y)$ are the displacements of the pore fluid and soil skeletal frame, and $e = \partial u_x/\partial x + \partial u_z/\partial z$ is the bulk strain of the skeletal frame of soil.

Because of the compressibility of the skeletal frame and pore water, there are three kinds of elastic waves propagating within the seabed. The first elastic waves are the fast compressional wave in which the solid skeletal and pore water move together. The second elastic waves are the slow compressional waves, which result from the seepage motion of the pore water relative to the moving solid skeletal frame. The last yet the most important elastic waves in the sea-seabed interactions are the shear waves.

Since we regard the soil as a linear medium, the three waves can be considered separately on the basis of superposition principle. Thus the displacement vectors of solid and pore fluid can be represented by the sum of two compressional waves and one shear wave:

$$\begin{aligned}\boldsymbol{u} &= \nabla\phi_f + \nabla\phi_s + \nabla\times\phi_T\hat{y},\\ \boldsymbol{w} &= \nabla\psi_f + \nabla\psi_s + \nabla\times\psi_T\hat{y},\end{aligned} \tag{2}$$

in which $\hat{y}$ is unit vector in the y-direction, the subscripts f, s, T represent fast, slow and shear

waves, respectively. Furthermore, since water wave is harmonic in both time and x-direction, the displacement in the soil is assumed to be also harmonic in both time and x-direction. That is to say, $\phi_{f,s,T}$, $\psi_{f,s,T}$ can be expressed in terms of $e^{i(\omega x - \tilde{k}x)}$. Putting $\psi_{f,s,T} = \tilde{c}_{f,s,T}\phi_{f,s,T}$, and substituting it into eq. (1), we have

$$\nabla^2\phi_{f,s,T} + \tilde{k}^2_{f,s,T}\,\phi_{f,s,T} = 0. \tag{3}$$

The general solution of eq. (3) is

$$\phi_{f,s,T} = [\tilde{a}_{1(f,s,T)}e^{\tilde{\lambda}_{f,s,T}z} + \tilde{a}_{2(f,s,T)}e^{-\tilde{\lambda}_{f,s,T}z}]e^{i(\omega t - \tilde{k}x)}, \tag{4}$$

where the six complex coefficients $\tilde{a}_{1,2(f,s,T)}$ and dispersion relation $(\tilde{k}, \omega)$ can be determined by the boundary conditions. The relations between $\tilde{\lambda}_{f,s,T}$, $\tilde{c}_{f,s,T}$, $\tilde{k}_{f,s,T}$ satisfy

$$\tilde{\lambda}^2_{f,s,T} = \tilde{k}^2 - \tilde{k}^2_{f,s,T},\quad \tilde{c}_{f,s} = \frac{\tilde{H} - \tilde{V}_{f,s}\rho}{\tilde{C} - \tilde{V}_{f,s}\rho_f},\quad \tilde{c}_T = -\frac{\rho_f}{\tilde{m}},$$

$$\tilde{k}^2_f + \tilde{k}^2_s = \frac{\omega^2(\tilde{H}\tilde{m} + \rho\tilde{M} - 2\rho_f\tilde{C})}{\tilde{H}\tilde{M} - \tilde{C}^2},\quad \tilde{k}^2_f\tilde{k}^2_s = \frac{\omega^4(\tilde{m}\rho - \rho_f^2)}{\tilde{H}\tilde{M} - \tilde{C}^2},$$

$$\tilde{k}^2_T = \frac{\omega^2(\rho - \rho_f^2/\tilde{m})}{\tilde{\mu}}.$$

With the above equations, we can define the wave velocities of the three elastic waves as

$$\tilde{V}_{f,s,T} = \omega/\tilde{k}_{f,s,T},$$

and the related Mach numbers can be written as

$$\tilde{M}a_{f,s,T} = \tilde{k}_{f,s,T}/\tilde{k}.$$

This is defined by the ratio of velocity of loading wave to velocity of elastic waves, representing the response of two compressional waves and one shear wave to water waves.

1.2 Boundary condition and solutions

At the water-soil interface, the boundary conditions are: (i) the vertical effective stress is zero, (ii) the fluid pressure is transmitted continuously from the sea to the pores in the seabed, and (iii) the mass of fluid must be conserved. Also, there is a boundary layer on the interface due to the shear stress, whose depth is of the same order as the diameter of the grain. Sawaragi[7] has demonstrated that the shear stress on the interface is much smaller than other stresses, even when the loading waves are strongly nonlinear. So we suppose that the shear stress is zero. The boundary conditions on the interface $z = 0$ then can be rewritten as

$$\tau_{zz} + p = 0,\quad p = -\rho_f\partial\varphi/\partial t,\quad \partial\varphi/\partial z = \partial u_z/\partial t + \partial w_z/\partial t,\quad \tau_{xz} = 0.$$

Assume that the bottom below a finite thickness $z = -d$ is impermeable and rigid:

$$u_x = 0,\quad u_z = 0,\quad w_z = 0.$$

Substituting the Biot's stress-strain relations and eq. (4) into the above equation yields the six coefficients $\tilde{a}_{1(f,s,T)}$, $\tilde{a}_{2(f,s,T)}$

$$\begin{bmatrix}\tilde{a}_{1f}\\ \tilde{a}_{2f}\\ \tilde{a}_{1s}\\ \tilde{a}_{2s}\\ \tilde{a}_{1T}\\ \tilde{a}_{2T}\end{bmatrix} = \begin{bmatrix} \tilde{r}_f & \tilde{r}_f & \tilde{r}_s & \tilde{r}_s & -i2\tilde{\mu}\tilde{k}\tilde{\lambda}_T & i2\tilde{\mu}\tilde{k}\tilde{\lambda}_T\\ -i2\tilde{\mu}\tilde{k}\tilde{\lambda}_f & i2\tilde{\mu}\tilde{k}\tilde{\lambda}_f & -i2\tilde{\mu}\tilde{k}\tilde{\lambda}_s & i2\tilde{\mu}\tilde{k}\tilde{\lambda}_s & -\tilde{\mu}(2\tilde{k}^2 - \tilde{k}_T^2) & -\tilde{\mu}(2\tilde{k}^2 - \tilde{k}_T^2)\\ (\tilde{M}\tilde{c}_f + \tilde{C})\tilde{k}_f^2 & (\tilde{M}\tilde{c}_f + \tilde{C})\tilde{k}_f^2 & (\tilde{M}\tilde{c}_s + \tilde{C})\tilde{k}_s^2 & (\tilde{M}\tilde{c}_s + \tilde{C})\tilde{k}_s^2 & 0 & 0\\ -i\tilde{k}e^{-\tilde{\lambda}_f d} & -i\tilde{k}e^{\tilde{\lambda}_f d} & -i\tilde{k}e^{-\tilde{\lambda}_s d} & -i\tilde{k}e^{\tilde{\lambda}_s d} & -\lambda_T e^{-\tilde{\lambda}_T d} & \lambda_T e^{\tilde{\lambda}_T d}\\ \tilde{\lambda}_f e^{-\tilde{\lambda}_f d} & \tilde{\lambda}_f e^{\tilde{\lambda}_f d} & \tilde{\lambda}_s e^{-\tilde{\lambda}_s d} & -\tilde{\lambda}_s e^{\tilde{\lambda}_s d} & -i\tilde{k}e^{-\tilde{\lambda}_T d} & -i\tilde{k}e^{\tilde{\lambda}_T d}\\ \tilde{c}_f\tilde{\lambda}_f e^{-\tilde{\lambda}_f d} & -\tilde{c}_f\tilde{\lambda}_f e^{\tilde{\lambda}_f d} & \tilde{c}_s\tilde{\lambda}_s e^{-\tilde{\lambda}_s d} & -\tilde{c}_s\tilde{\lambda}_s e^{\tilde{\lambda}_s d} & -i\tilde{k}\tilde{c}_T e^{-\tilde{\lambda}_T d} & -i\tilde{k}\tilde{c}_T e^{\tilde{\lambda}_T d} \end{bmatrix}^{-1}\begin{bmatrix}0\\0\\-\rho_f\dfrac{\partial\varphi}{\partial t}\\0\\0\\0\end{bmatrix},$$

And the dispersion relation can be obtained

$$th(\tilde{k}h) = \frac{\omega^2}{g\tilde{k}}\left[1 - \frac{w_z(0) + u_z(0)}{a_0 \cosh \tilde{k}h}\right],$$

where $\tilde{r}_{f,s} = \tilde{k}^2_{f,s}[(\tilde{C} - \tilde{H}) + (\tilde{M} - \tilde{C})\tilde{c}_{f,s}] + 2\tilde{\mu}\tilde{k}^2$. So the displacements of the soil skeletal frame and pore fluid, the pore pressure and the total stress components are derived as

$$\begin{aligned}
u_x &= \{(-\tilde{a}_{1f}e^{\tilde{\lambda}_f Z} - \tilde{a}_{2f}e^{-\tilde{\lambda}_f Z} - \tilde{a}_{1s}e^{\tilde{\lambda}_s Z} - \tilde{a}_{2s}e^{-\tilde{\lambda}_s Z})i\tilde{k} + (-\tilde{a}_{1T}e^{\tilde{\lambda}_T Z} \\
&\quad + \tilde{a}_{2T}e^{-\tilde{\lambda}_T Z})\tilde{\lambda}_T\}e^{i(\omega t - \tilde{k}x)}, \\
u_z &= \{(\tilde{a}_{1f}e^{\tilde{\lambda}_f Z} - \tilde{a}_{2f}e^{-\tilde{\lambda}_f Z})\tilde{\lambda}_f + (\tilde{a}_{1s}e^{\tilde{\lambda}_s Z} - \tilde{a}_{2s}e^{-\tilde{\lambda}_s Z})\tilde{\lambda}_s + (-\tilde{a}_{1T}e^{\tilde{\lambda}_T Z} \\
&\quad - \tilde{a}_{2T}e^{-\tilde{\lambda}_T Z})i\tilde{k}\}e^{i(\omega t - \tilde{k}x)}, \\
w_x &= \{(-\tilde{a}_{1f}e^{\tilde{\lambda}_f Z} - \tilde{a}_{2f}e^{-\tilde{\lambda}_f Z})\tilde{c}_f i\tilde{k} + (-\tilde{a}_{1s}e^{\tilde{\lambda}_s Z} - \tilde{a}_{2s}e^{-\tilde{\lambda}_s Z})\tilde{c}_s i\tilde{k} \\
&\quad + (-\tilde{a}_{1T}e^{\tilde{\lambda}_T Z} + \tilde{a}_{2T}e^{-\tilde{\lambda}_T Z})\tilde{c}_T\tilde{\lambda}_T\}e^{i(\omega t - \tilde{k}x)}, \\
w_z &= \{(\tilde{a}_{1f}e^{\tilde{\lambda}_f Z} - \tilde{a}_{2f}e^{-\tilde{\lambda}_f Z})\tilde{c}_f\tilde{\lambda}_f + (\tilde{a}_{1s}e^{\tilde{\lambda}_s Z} - \tilde{a}_{2s}e^{-\tilde{\lambda}_s Z})\tilde{c}_s\tilde{\lambda}_s \\
&\quad + (-\tilde{a}_{1T}e^{\tilde{\lambda}_T Z} - \tilde{a}_{2T}e^{-\tilde{\lambda}_T Z})\tilde{c}_T i\tilde{k}\}e^{i(\omega t - \tilde{k}x)}, \\
p &= \{(\tilde{a}_{1f}e^{\tilde{\lambda}_f Z} + \tilde{a}_{2f}e^{-\tilde{\lambda}_f Z})[\tilde{C} + \tilde{c}_f\tilde{M}]\tilde{k}^2_f + (\tilde{a}_{1s}e^{\tilde{\lambda}_s Z} + \tilde{a}_{2s}e^{-\tilde{\lambda}_s Z})[\tilde{C} + \tilde{c}_s\tilde{M}]\tilde{k}^2_s\}e^{i(\omega t - \tilde{k}x)}, \\
\tau_{xx} &= \{(-\tilde{a}_{1f}e^{\tilde{\lambda}_f Z} - \tilde{a}_{2f}e^{-\tilde{\lambda}_f Z})[(\tilde{H} + \tilde{c}_f\tilde{C})\tilde{k}^2_f + 2\tilde{\mu}\tilde{\lambda}^2_f] + (-\tilde{a}_{1s}e^{\tilde{\lambda}_s Z} - \tilde{a}_{2s}e^{-\tilde{\lambda}_s Z}) \\
&\quad [(\tilde{H} + \tilde{c}_s\tilde{C})\tilde{k}^2_s + 2\tilde{\mu}\tilde{\lambda}^2_s] + (\tilde{a}_{1T}e^{\tilde{\lambda}_T Z} - \tilde{a}_{2T}e^{-\tilde{\lambda}_T Z})2i\tilde{\mu}\tilde{k}\tilde{\lambda}_T\}e^{i(\omega t - \tilde{k}x)}, \\
\tau_{zz} &= \{(-\tilde{a}_{1f}e^{\tilde{\lambda}_f Z} - \tilde{a}_{2f}e^{-\tilde{\lambda}_f Z})[(\tilde{H} + \tilde{c}_f\tilde{C})\tilde{k}^2_f - 2\tilde{\mu}\tilde{k}^2] + (-\tilde{a}_{1s}e^{\tilde{\lambda}_s Z} - \tilde{a}_{2s}e^{-\tilde{\lambda}_s Z}) \\
&\quad [(\tilde{H} + \tilde{c}_s\tilde{C})\tilde{k}^2_s - 2\tilde{\mu}\tilde{k}^2] + (-\tilde{a}_{1T}e^{\tilde{\lambda}_T Z} + \tilde{a}_{2T}e^{-\tilde{\lambda}_T Z})2i\tilde{\mu}\tilde{k}\tilde{\lambda}_T\}e^{i(\omega t - \tilde{k}x)}, \\
\tau_{xz} &= \{(-\tilde{a}_{1f}e^{\tilde{\lambda}_f Z} + \tilde{a}_{2f}e^{-\tilde{\lambda}_f Z})2i\tilde{\mu}\tilde{k}\tilde{\lambda}_f + (-\tilde{a}_{1s}e^{\tilde{\lambda}_s Z} + \tilde{a}_{2s}e^{-\tilde{\lambda}_s Z})2i\tilde{\mu}\tilde{k}\tilde{\lambda}_s \\
&\quad + (-\tilde{a}_{1T}e^{\tilde{\lambda}_T Z} - \tilde{a}_{2T}e^{-\tilde{\lambda}_T Z})(2\tilde{k}^2 - \tilde{k}^2_T)\tilde{\mu}\}e^{i(\omega t - \tilde{k}x)}.
\end{aligned}$$

Since the above solutions are based on the slightly non-elastic model and principle of superposition, they are valid for studying dynamic response of varied marine soils on the condition of small bed deformation.

2 Numerical results and analysis

2.1 The experiments of resonance and calculating parameters

A soil basin with dimension of 3 m × 0.9 m × 0.6 m was equipped inside a 54.8 m × 2.4 m × 1.5 m experimental wave flume. The pore pressures were measured on both sand and silt seabed with varying loading waves and consolidation periods. It has been found[3] that (i) in the fresh silt seabed, there was sometimes a clear resonance and at other times non-resonance, and the resonance events present were localized; (ii) there are major discrepancies between preresonated soil and fresh silt. One apparent difficulty is that the preresonated soil was very weak and a reloading on such soil will cause a quick and significant fluidization, but the fresh silt is relatively stable and responds almost linearly to loading waves similar to coarse sand seabed before being resonated. For convenience of comparison, some experimental data of Foda[3] and Tzang is provided in table 1. The experiments used fresh soil which had not experienced a resonance fluidization response earlier. Clearly, all of the experiments can be separated into three cases: case 1, the seabed is of the silt type, the resonance event is observed, for example, tests 2, 4, and 14; case 2, the soil is also the silt, but non-resonance is observed, for example, tests 3, 15; case 3, the soil is coarse sand and non-resonance, for example, test No.11. In order to study the mechanism of such a resonance, this paper focuses on the pre-resonance silty response. The

soil parameters used in the present paper are tabulated in table 2.

Table 1 Experimental results of Foda and Tzang

Test series	Wave heigh H/cm	Wave period T/s	Soil	Resonance	Initial resonant depth/m	Mean pore pressure/ kN·m^{-2}
2	8.3	1.72	Silt	Yes	0.203	1.416
3	10.2	1.7	Silt	No		0.163
4	7.0	1.98	Silt	Yes	0.203	1.456
11	7.5	1.97	Sand	No		0.172
14	10.7	1.51	Silt	Yes	0.203	1.571
15	10.3	1.51	Silt	No		0.150

Table 2 Numerical parameters of soil

Name of soil parameters	Sand	Silt 1	Silt 2
Porosity	0.4	0.494 ~ 0.525	0.45
Poisson's ratio	0.35	0.49	0.4
Shear modulus G(N·m^{-2})	10^7	$10^5 \sim 10^6$	10^6
Permeability K_s(m^3·s/kg)	4×10^{-8}	10^{-11}	10^{-11}
Viscosity of pore water η_f(Kg/m·s)	10^{-3}	10^{-3}	10^{-3}
Added mass of skeletal frame α	0.25	0.25	0.25
Bulk modulus of pore water K_f(N/m)	1.92×10^9	1.92×10^9	1.92×10^9
Bulk modulus of grain material K_r(N/m)	3.6×10^{10}	3.6×10^{10}	3.6×10^{10}
Density of pore water ρ_f(kg/m^3)	1.03×10^3	1.03×10^3	1.03×10^3
Density of grain material ρ_r(kg/m^3)	2.61×10^3	2.61×10^3	2.61×10^3
Coulomb loss δ	0.05	0.05	0.05
Saturation Sr	0.99	0.99	0.99

First of all, we analyze the test results. By definition, as the soil particles are in a state of suspension with their weights entirely supported by pore pressure, the soil is fluidized; that is, $\Delta p = (1-\beta)(\rho_r - \rho_f)gz$. By this relation, if the value of $\Delta p > 1.539$ kN/m^2 at depth $z = -0.203$ m, liquefaction occurs. Thus, the maximum of pore pressure in tests 2, 4, and 14 is about 1.8 kN/m^2, enough to fluidize the layer of seabed, and in tests 3 and 15, the seabed remaihs approximately stable (see (1) of ref. [3]). Based on the principle of limiting equilibrium, the estimated value of failure depth was about 0.05 m and below this depth the seabed was stable. That is to say, the cause of seabed instability could not be explained by this principle and should be considered by the physical properties of the silt seabed.

Table 1 shows that the soil used in all of the tests is silt except for test 11, and the discrepancy of loading wave periods is small. A comparison of test 2 and test 3, for example, indicated that the difference is only 0.02 s, which can be neglected, and the major discrepancy between the two tests is the wave height, 1.9 cm. Larger waves should cause nonlinear waves effects, and thus the theory of linear waves may be invalid when wave height increases. Generally speaking, as $kh = O(1)$, the linear condition is $ka_0 \ll 1$. With the previous dispersion relation, we obtain

Test 2: $k_r h = 0.657$, $k_r a_0 = 0.1087$,

Test 3: $k_r h = 0.670$, $k_r a_0 = 0.1357$.

The above results indicate that it suffices to consider the effects of linear loading waves on the seabed. We suggest that the cause of a non-resonance event in test 3 is not owing to the nonlinearity of wave influence upon the seabed, but to the dynamic response of the soil to the waves. This conclusion can also be obtained from tests 14 and 15. The loading conditions over the bed

are almost the same but the results are oppisite.

In the following sections, we will discuss further the main characteristics of soil inside the seabed under water wave loading, using the soil parameters of silt 1 and silt 2, under the same wave conditions as tests 2, 3, and 11.

2.2 Distribution of pore pressures and stresses

First, we give a description of the distribution of the pore pressure $|p|/p_B$ response inside the coarse sand and silt seabed (p_B is the value of pressure p at the interface). As shown in fig. 1, in the silt seabed the pore pressure near the seabed surface decreases significantly and then it varies slowly after some depth, but the pore pressure in the coarse sand bed varies continually with depth and responds to the wave loading linearly. In order to verify the present theory and parameters of the marine soil, fig. 1 also shows the measurements of pre-resonance pore pressure oscillation. Good is the agreement between theory and observation. Clearly, the present model and soil parameters are valid.

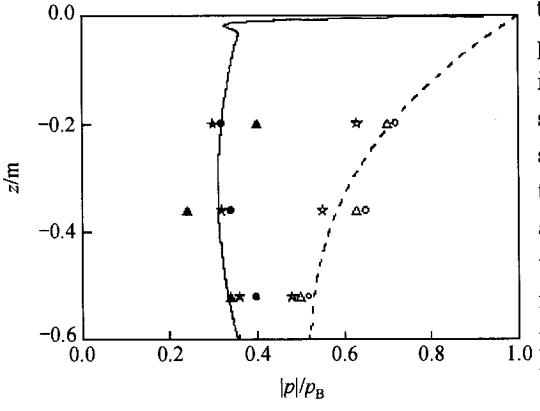

Fig. 1. Distribution of pore pressure. —, Silty sand; - - - -, coarse sand; ● and ○, t = 30s for silty sand and coarse sand respectively; ☆, ★, t = 35s; ▲, △, t = 40s.

The plots of dimensionless stresses versus the seabed depth are described in fig. 2. We notice that profile of effective shear stress $|\tau'_{xz}|/p_B$ in coarse sand is similar to that in silt. But the vertical distributions of effective normal stresses in z-direction have significant differences. Firstly, the $|\tau'_{zz}|/p_B$ in the silt is greater than that in coarse sand, and reaches the maximum near the water-soil interface, and decreases gradually thereafter. The $|\tau'_{zz}|/p_B$ in a coarse sand increases as z/h increases, and reaches the maximum value at $z = -0.42$ m and then decreases. Secondly, the curve of effective normal stress $|\tau'_{xx}|/p_B$ in x-direction in silt bed is different from that in coarse sand. The variation in $|\tau'_{xx}|/p_B$ with depth is non-monotonic, and approaches zero at $z = -0.04$ m and $z = -0.42$ m, and there is a peak at $z = -0.2$ m. For a coarse sand bed, the $|\tau'_{xx}|/p_B$ monotonically decreases in the depth range from $z = 0.0$m to $z = -0.55$ m, except for the value around the bottom of seabed $z = -d$.

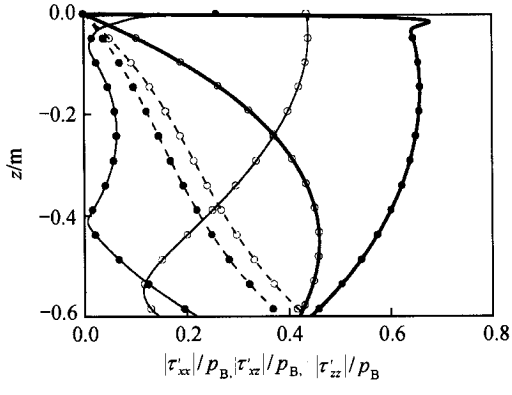

Fig. 2. The distribution of stresses. —, $|\tau'_{zz}|/p_B$; —, $|\tau'_{xx}|/p_B$; ----, $|\tau'_{xz}|/p_B$; ●, sand; ○, course sand.

2.3 Angle of stresses

In order to understand the distribution of stresses within a seabed, we further analyze the profile of stress angle in the region of a wavelength. According to the traditional sign convention for stresses, a stress is positive when it acts as compression. The total effective stresses and shear stress are written as

$$\bar{\tau}_{xx} = \tau_{x0} - \tau'_{xx} = -(\gamma_s - \gamma_f)K_0 z - \tau_{xx} - p,$$
$$\bar{\tau}_{zz} = \tau_{z0} - \tau'_{zz} = -(\gamma_s - \gamma_f)z - \tau_{zz} - p,$$
$$\bar{\tau}_{xz} = -\tau_{xz},$$

where τ_{z0}, τ_{x0} are the effective stresses at initial equilibrium in the z- and x-direction, respectively; τ'_{xx}, τ'_{zz} are the effective normal stress in x- and z-direction, γ_s, γ_f are the unit weight of soil and water, K_0 is a coefficient of earth pressure at rest, ranging from 0.4 to 1.0, and is related to the Poisson ratio, and ν is given by $K_0 = \frac{\nu}{1-\nu}$. The stresses at a given location may be conveniently expressed by the stress angle ϑ:

$$\sin\vartheta = \frac{\sqrt{(\bar{\tau}_{xx} - \bar{\tau}_{zz})^2 + 4\bar{\tau}_{xz}^2}}{(\bar{\tau}_{xx} + \bar{\tau}_{zz})}.$$

The distribution of $\vartheta(x, z, t)$ only in the region of a wavelength is shown in fig. 3, in which $x/L = 0$ represents the location of the wave crest and $x/L = 0.5$ represents the location of the wave trough. The state of stress can be deduced by the stress angle. As we know, every kind of soil has an angle of internal friction, ϑ_f, which depends on the soil type. Once $\vartheta(x, z, t) \geqslant \vartheta_f$, the seabed fails. In general, the ϑ_f for coarse sand ranges from 32° to 40° and from 28° to 36° for silt or fine sand. The results of the present study suggest that the stress angles decrease as the depth increases with the maximum values close to the interface. To express the state of stresses effectively, we only depicted the contours from 0° to 45° (fig. 3). In fig. 3(a), the distribution of stress angles for silt 1 is almost symmetrical with the period 2 times that of water waves. This is especially pronounced at the top portion of the bed. But for the soils, silt 2 and sand, the distribution of stress angles are asymmetrical . For the silt 2 bed , in the same depth the angle at

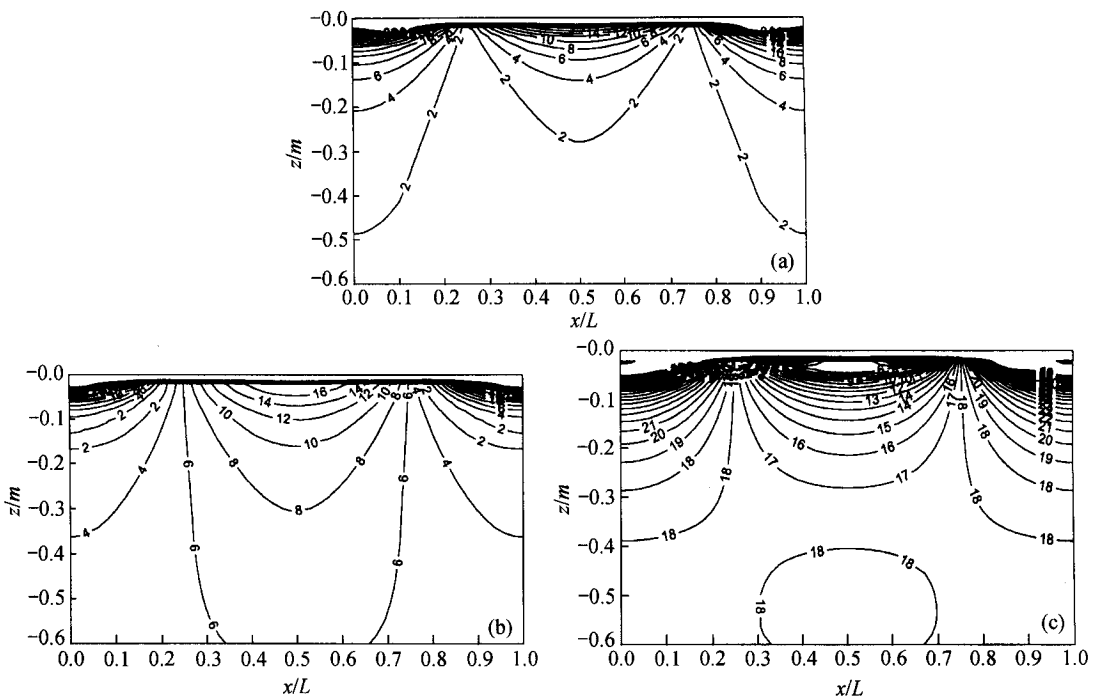

Fig. 3. The distribution of the effective stresses in terms of the stress angle in the seabed. (a) Silt 1; (b) silt 2; (c) sand.

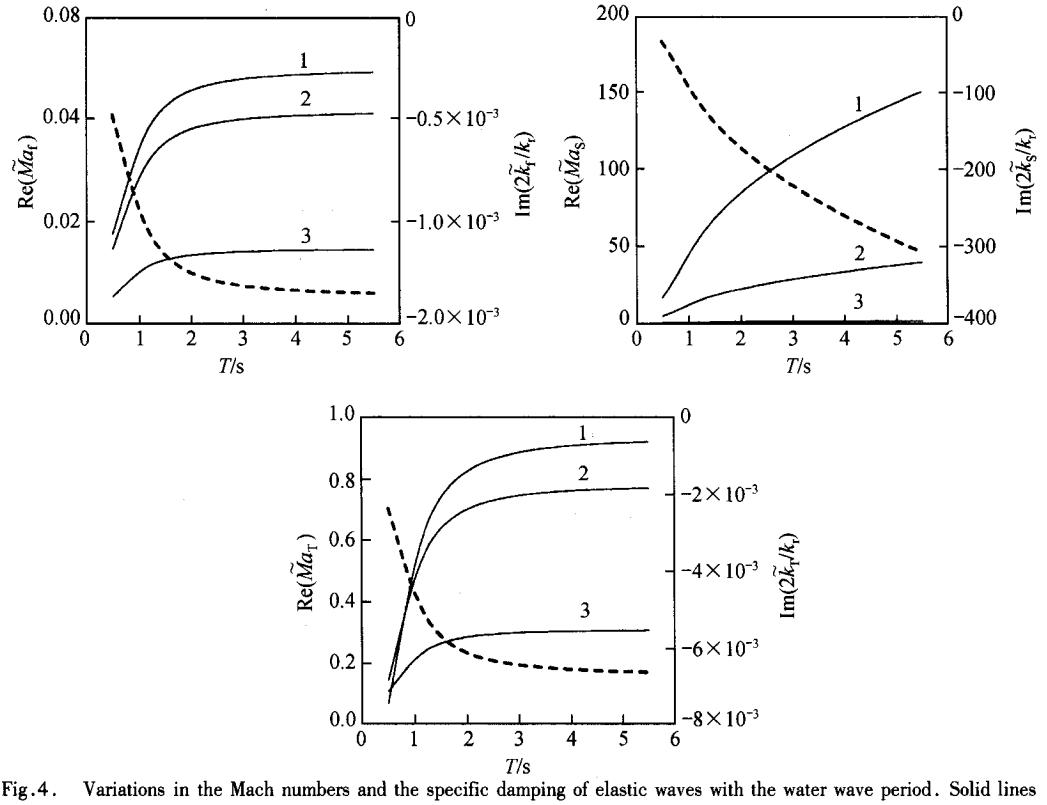

Fig.4. Variations in the Mach numbers and the specific damping of elastic waves with the water wave period. Solid lines 1, 2, 3 are corresponding to silt 1, silt 2, sand, respectively; dashed lines are damping curves only for silt 1.

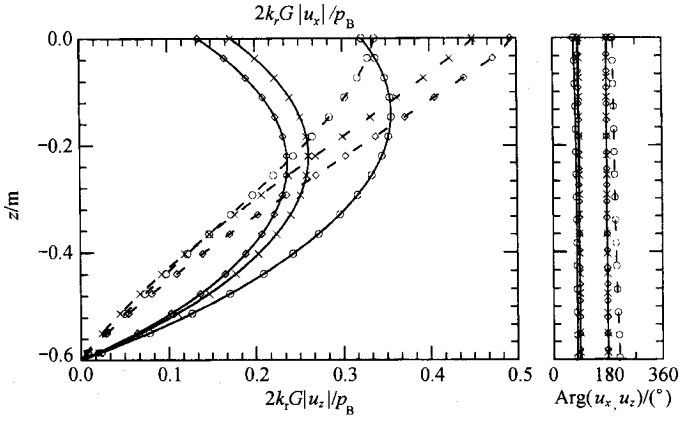

Fig. 5. Vertical distribution of soil skeletal frame and its phase. Perpendicular displacements in solid line; horizontal displacements in dashed line; ×, silt 1; □, silt 2; ○, sand.

the wave trough is larger than that at the wave crest, but the reverse is found for sand bed. This implies that the stresses are more uniformly distributed in silt 1 bed.

2.4 Elastic waves

The real parts of the three Mach numbers and the imaginary parts of elastic for the silt versus T are plotted in figs. 4—6. All of the Mach numbers increases with the period of water waves,

and as $T > 2$s, $\mathrm{Re}(\widetilde{M}a_f)$ and $\mathrm{Re}(\widetilde{M}a_T)$ are invariant with period. From the definition of Mach number, it should be known that the velocity of the fast compressional waves is much higher than the phase velocity of the water waves, especially for the sand bed, in the order of $\mathrm{Re}(\widetilde{M}a_f) \sim 10^{-2}$. The velocity of the slow compressional waves, however, is significantly lowered compared to the phase speed of the water waves, and the slow compressional waves are highly damped by the viscosity of pore fluid. The velocity of the shear waves keeps the same order as the speed of water waves. As the period of water waves is 1.7 s, $\mathrm{Re}(\widetilde{M}a_T$ is 0.78 for silt 1, 0.67 for silt 2, and 0.27 for sand. Consequently, we conclude that the shear waves are one of the main causes of resonance.

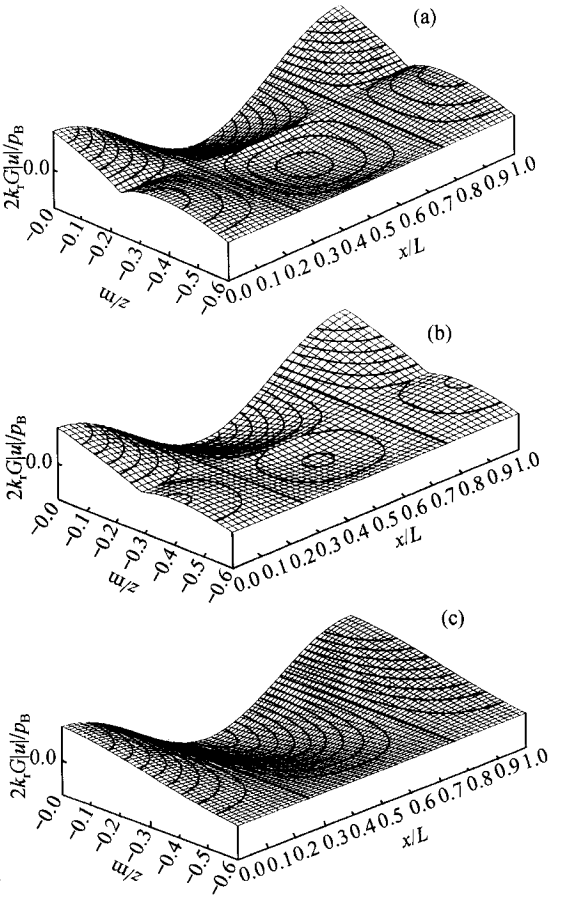

Fig. 6. 3D distribution of soil skeletal frame. (a) Silt 1; (b) silt 2; (c) sand.

2.5 Displacement of soil skeletal frame and pore fluid

The amplitudes of distribution of the horizontal and perpendicular displacements and their phases, varying with depth, of the soil skeletal frame are given in fig. 5. There is essentially no difference in the responses to water waves of the sandy and silt beds shown by the curves. However, it is clear that the 3-dimensional displacements of soil skeletal frame for both the sand bed and the silt bed are different (fig. 6). In the sand bed, the 3-dimensional distribution of displacement is even, and in the silt-1 seabed the bed is divided into two parts: one part ranges from $-0.02\ \mathrm{m} < z < 0.0$ m and the other from $-0.6\ \mathrm{m} < z < -0.02$ m. It is clear that at $z = -0.02$ m the marine sediment has almost no motion, i.e. there is a hardened layer inside the bed. Similar behavior was found in silt 2 but the locality of the layer is a little different, suggesting that a stiffness layer in a silt bed can cause abnormal events. This is also observed by experiments[3].

For the purposes of analyzing the effect of wave parameters on a stiffness layer, we chose two groups, tests 4 and 14, and found that the location of the stiffness layer is almost stable. It is then concluded that the location mainly depends on the properties of the soil. We consider the effect of the thickness of seabed on the stiffness layer for three cases: $d = -0.6$ m, -1.0 m, -2.0 m. The thicker the soil, the deeper the stiffness layer (fig. 7), and when $z = -2.0$, the stiffness layer no longer exists, i.e. whether the stiffness layer exists or not is related to the thickness of the seabed.

On the other hand, we now turn back to the distribution of displacement of pore fluid and its phases (fig. 8). The vertical displacement descends rapidly near water-soil surface, and it ap-

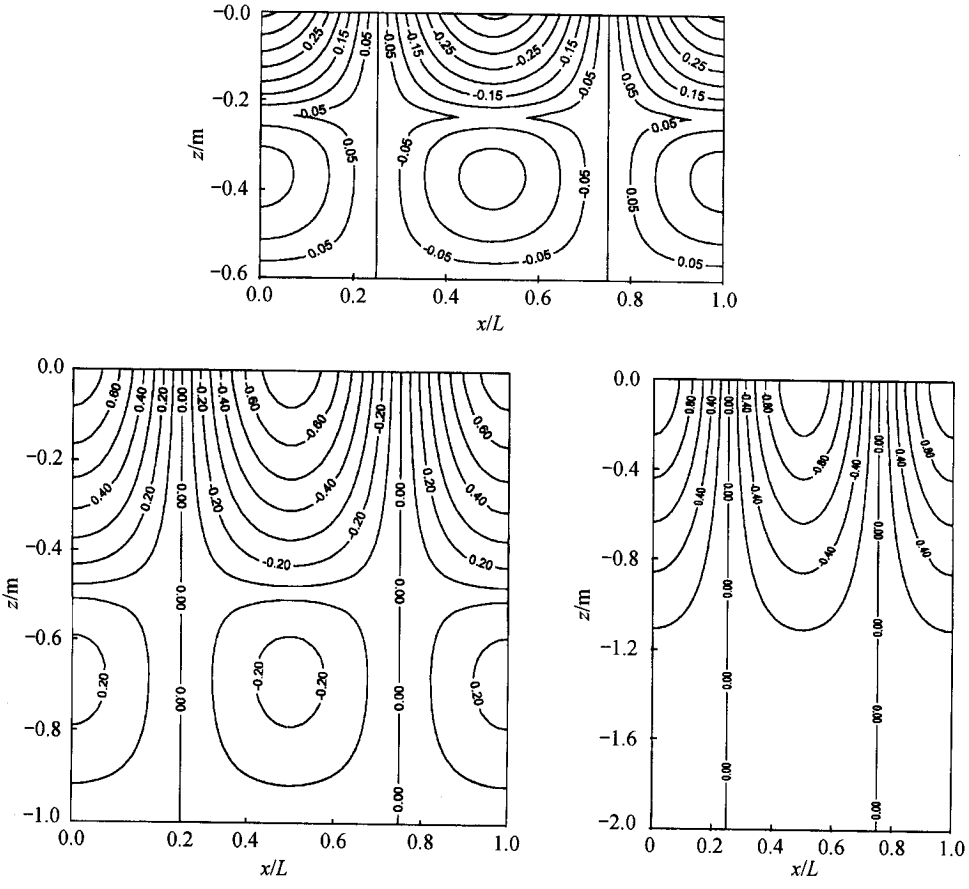

Fig. 7. The contours of soil skeletal frame displacement in the region of a wavelength for $d = -0.6$ m, -1.0 m, -2.0 m.

proaches zero at $z = -0.2$ m, and then the phase reverses. This is because of the existence of a stiffness layer which makes the pore fluid break. As expected, the distribution of sand bed declines gradually. Foda and Tzang have measured the changes in soil stiffness. and observed that there was sometimes an anomalous layer at mid-depth of a significantly hardened soil, with a surprisingly high resistance to penetration. Their results are in accord with ours.

2.6 Analysis of resonance

As is obvious in the above analysis, the responses of sand beds and silt beds to water waves are different. Particularly, in the silt seabed, the velocity of shear waves approaches the speed of water waves, and there was a stiffness layer in the soil, with no motion of the soil skeletal frame and the reverse for the pore fluid. Fig. 6 shows the displacement contours of soil skeletal frame. It also indicates that at the location of a "channel", which is filled with a mixture of pore fluid and soil particles, there are some cavities. When the water waves act on the silt seabed continuously, the solid particles are surrounding the soil skeleton with weak cohesion dropping under vibrating stresses. This caused two results: one is that the "channel" has been widened and the other is the soil particle portion of pore fluid increased. By the definition of inherence frequency, we know that the inherence frequency of a cavuum is in inverse proportion to its volume and mass. Therefore both results reduced the inherence frequency of the "channel". We suggest that

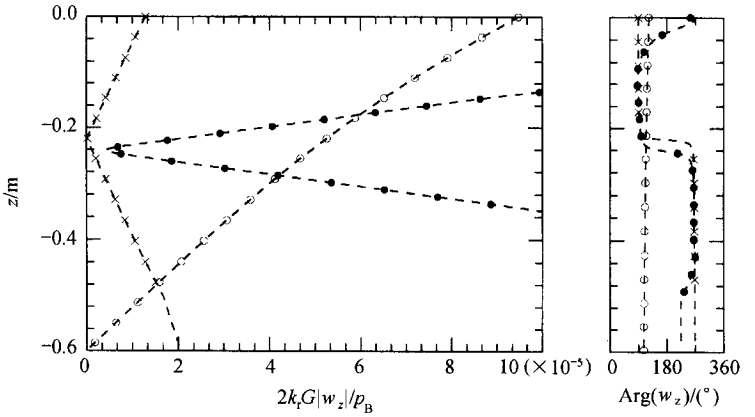

Fig. 8. Vertical distribution of perpendicular displacement of pore fluid and its phase. ×, Silt 1; ●, silt 2; ○, sand.

only when the inherence frequency of "channel" is close to that of water waves would resonance occur at the stiffness layer. In Foda's experiment, the depth of resonant soil fluidization was at $z = -2.03$ m, differing from the numerical solution only by 0.03 m. The results of present theory are thus in good agreement with the experimental data. With regard to the other two non-resonant experiments No. 3 and No. 15, the soil used might probably be a little harder than others and could not form "channel" in the bed.

In brief, we propose that the existence of the stiffness layer is an essential condition for the resonance to occur. Only when the stiffness layer exists and the frequency of shear waves is close to the frequency of water waves, will resonance occur. When the seabed is rather thick, there is no possibility for resonance to take place inside the soil bed. Therefore, resonance in the shallow silt seabed may cause the partial suspension of soil particles and seabed sinking. Since the soil inner structures are very complex especially for silt, the above conclusion should be validated by practical engineering.

3 Conclusions

In this paper, the dynamic properties of soil for a finite thickness bed induced by linear loading waves is treated analytically with the weak non-elastic media model. By analyzing the silt properties before resonance, the mechanism for resonance is discussed in detail. Some conclusions can be drawn as follows.

(1) In consideration of interaction of water waves and soil, the pore pressure in silt seabed is only a small fraction of the bottom pressure amplitude. The softer the soil, the more symmetric the distribution of stresses.

(2) As the order of elastic moduli is about 10^5 and the depth of seabed $d \ll L$, a stiffness layer might be formed within silt seabed. Moreover the existence of a stiffness layer is an essential condition for forming a channel. As $d \gg L$, the stiffness layer disappears.

(3) Whether resonance occurs depends on the velocity of the shear waves and the value of the elastic moduli. In the presence of stiffness layer, only when the velocity of the shear waves approaches the speed of water waves will resonance occur.

Acknowledgements This work was supported by the National Natural Science Foundation of China (Grant No. 19602021).

References

1. Goddard, J. D., Nonlinear elasticity and pressure dependent wave speeds in granular media, Proc. R. Soc. Lond., 1990, 430: 105—131.
2. Bennett, R. H., *In situ* porosity and permeability of selected carbonate sediment: Great Bahama 1. Measurements, Marine Geotechnology, 1990, 9: 1—28.
3. Foda, M. A., Resonant fluidization of silty soil by water waves, J. G. R., 1994, 99(10): 20264—20475.
4. Yamamoto, T., Koning, H. L., Sellmeijer, H., et al., On the response of a poro-elastic bed to water waves, J. F. M., 1978, 87: 193—206.
5. Li, J. C., Lin, M., On the interaction of water waves and seabed by porous medium model, Acta Mechanics Sinica, 1995, 11(2): 17—27.
6. Biot, M. A., Mechanics of deformation and acoustic propagation in porous media, J. Appl. Phys., 1962, 33: 1482—1498.
7. Sawaragi, T., Deguchi, I., Wave on permeable layers, Proc. 23rd Int. Conf. Coastal Eng., ASCE, 1992, 1531—1544.